Critical behavior of the Anderson transition in higher-dimensional Bogoliubov–de Gennes symmetry classes

Tong Wang [1,2,*] Zhiming Pan,[3,†] Keith Slevin [4] and Tomi Ohtsuki [5]

[1]*International Center for Quantum Materials, School of Physics, Peking University, Beijing 100871, China*
[2]*Collaborative Innovation Center of Quantum Matter, Beijing 100871, China*
[3]*Institute for Theoretical Sciences, Westlake University, Hangzhou 310024, Zhejiang, China*
[4]*Department of Physics, Osaka University, Toyonaka, Osaka 560-0043, Japan*
[5]*Physics Division, Sophia University, Chiyoda-ku, Tokyo 102-8554, Japan*

(Received 7 July 2023; revised 11 October 2023; accepted 12 October 2023; published 30 October 2023)

Disorder is ubiquitous in solid-state systems and its crucial influence on transport properties was revealed by the discovery of Anderson localization. Generally speaking, all bulk states will be exponentially localized in the strong disorder limit, but whether an Anderson transition takes place depends on the dimension and symmetries of the system. The scaling theory and symmetry classes are at the heart of the study of the Anderson transition, and the critical exponent ν characterizing the power-law divergence of localization length is of particular interest. In contrast with the well-established lower critical dimension $d_l = 2$ of the Anderson transition, the upper critical dimension d_u, above which the disordered system can be described by mean-field theory, remains uncertain and precise numerical evaluations of the critical exponent in higher dimensions are needed. In this study, we apply the Borel-Padé resummation method to the known perturbative results of the nonlinear sigma model to estimate the critical exponents of the Bogoliubov–de Gennes classes. We also report numerical simulations of class DIII in three dimensions, and classes C and CI in four dimensions, and compare the results of the resummation method with these and previously published work. Our results may be experimentally tested in realizations of quantum kicked rotor models in atomic-optic systems, where the critical behavior of dynamical localization in higher dimensions can be measured.

DOI: 10.1103/PhysRevB.108.144208

I. INTRODUCTION

Since the discovery of Anderson localization [1], the effects of disorder in various media have been a constant focus of the physics community. The disorder-driven Anderson transition (AT) is a second-order quantum phase transition, around which physical observables show universal power-law behaviors. The universality class of the AT depends on the dimensionality and fundamental symmetries of the system: time-reversal symmetry, particle-hole symmetry, and chiral symmetry [2–4]. Based on these symmetries, Altland and Zirnbauer (AZ) completed the symmetry classification of noninteracting disordered Hamiltonians known as the "10-fold way" [5]. The classification is comprised of the three Wigner-Dyson classes (A, AI, and AII), the three chiral classes (AIII, BDI, and CII), and the four Bogoliubov–de Gennes (BdG) classes (D, C, DIII, and CI). The AZ classification is revelatory not only to the study of localization phenomena, but to the study of topological materials [6–8].

The critical exponent ν of the AT characterizes the power-law divergence of the correlation length ξ on approaching the critical point,

$$\xi \sim |x - x_c|^{-\nu}, \tag{1}$$

where x is the tuning parameter and x_c is the critical point. Constrained by computational capacity, relatively few numerical studies have gone beyond three dimensions (3D) [9–13] into higher dimensions, where a stronger strength of disorder is required to drive the system into localization. A strong-disorder renormalization group (RG) approach is in development to provide theoretical insights [14,15]. Recently, the potentials of such efforts are revealed by the proposed superuniversality of ATs in Hermitian and non-Hermitian systems [16], and the mapping between certain disorder-free interacting systems and disordered noninteracting systems with extra dimension [17,18]. On the other hand, the quantum kicked rotor model had been related to the Anderson localization problem [19–22], with the incommensurate frequencies of periodical kicks substituting the role of spatial dimensions [20,23–27]. Experimental proposals and realizations of the the quantum kicked rotor model in cold-atom systems point to a promising test bed for theoretical and numerical results of Anderson localization in higher dimensions [28].

While the lower critical dimension $d_l = 2$ of the AT is well established by the one-parameter scaling theory [3], the upper critical dimension d_u, above which a mean-field description is accurate, remains debatable. The self-consistent theory of AT

*wangtong617@pku.edu.cn
†panzhiming@westlake.edu.cn

by Vollhardt and Wölfle [29,30] gives the critical exponent of the Anderson model (class AI) as

$$\nu = \begin{cases} \dfrac{1}{d-2}, & 2 < d < 4 \\ \dfrac{1}{2}, & d \geqslant 4. \end{cases} \tag{2}$$

The results of $d_u = 4$ and the mean-field critical exponent $\nu = 1/2$ are reminiscent of the ϕ^4 theory. A modified version of this theory that considers the renormalization of the diffusion coefficient [9] gives

$$\nu = \frac{1}{2} + \frac{1}{d-2}, \tag{3}$$

and $d_u = \infty$. The prediction of the limiting value

$$\lim_{d\to\infty} \nu = \tfrac{1}{2}, \tag{4}$$

by both theories, agree with the value from the Anderson model on an infinite-dimensional Bethe lattice [31–37]. However, Eq. (3) is in better agreement with the numerical results [11,38–40] of the orthogonal symmetry class for $d = 3, 4, 5, 6$ than Eq. (2).

On the other hand, the nonlinear sigma model (NLσM), an effective field theory of Anderson localization, has been studied extensively in $d = 2 + \epsilon$ dimensions [41–44]. The β function, which describes the renormalization of the conductance with system size, can be calculated analytically using perturbation techniques [45–48]. From the β function, one can derive relevant physical quantities including a series in powers of ϵ for the critical exponent ν. This method, which is referred to as the ϵ expansion, is rigorous only when $\epsilon \ll 1$. In this limit, the ϵ expansion gives $\nu = 1/\epsilon$, in agreement with Eq. (2), but not Eq. (3), and with numerical simulations on fractals with spectral dimensions close to 2 [38,49]. To obtain results for higher dimensions, resummation methods are needed. However, a straightforward resummation [44] of the power series for the critical exponent yields $\nu \to 0$ in the limit $d \to \infty$, in disagreement with both Eqs. (2) and (3). For the Wigner-Dyson classes, resummations that incorporate the correct asymptotic behavior of the critical exponent for $d \to \infty$ have been performed [11,50], giving better agreement with numerical simulations [11,12,39,40] and experimental results [26,27]. However, a comprehensive understanding of the dimensional dependence of the AT in different symmetry classes is still lacking.

In this paper, we focus on the BdG symmetry classes in 3D and 4D. The four BdG classes appear naturally in the topological superconductors (SCs) [4,5]. The underlying BdG Hamiltonian H is invariant under the antiunitary transform of particle-hole symmetry (PHS) $\mathcal{C} = U_C K$,

$$\mathcal{C}: \quad H \to -U_C^{\dagger} H^T U_C, \tag{5}$$

where U_C is a unitary matrix and K denotes the operation of complex conjugation [8]. The BdG universality classes are realized at the particle-hole symmetric point, $E = 0$. The particle-hole symmetry can be classified into two kinds: even ($\mathcal{C}^2 = +1$) or odd ($\mathcal{C}^2 = -1$). SCs with these two kinds of particle-hole symmetry can be further classified according to time-reversal symmetry (TRS) $\mathcal{T}$. There are four BdG classes corresponding to different types of SCs: singlet/triplet SC (class D), singlet SC (class C), singlet/triplet SC with TRS (class DIII), and singlet SC with TRS (class CI). Class D and class C describe BdG systems with even or odd PHS and broken TRS. Classes DIII and CI are characterized by a time-reversal operator $\mathcal{T}: H \to U_T H^T U_T^{-1}$, where the unitary matrix U_T satisfies $U_T^2 = \pm 1$. For classes DIII, one has PHS $\mathcal{C}^2 = +1$ and TRS $\mathcal{T}^2 = -1$. For class CI, one has PHS $\mathcal{C}^2 = -1$ and TRS $\mathcal{T}^2 = +1$. The symmetries of the BdG classes are summarized in Table I. Due to the absence of spin-rotation invariance, class D and class DIII exhibit weak antilocalization.

Below we apply the resummation method previously employed [11,50] for the Wigner-Dyson symmetry classes to the BdG classes. We also report simulations using the transfer matrix method for class DIII in 3D, and classes C and CI in four dimensions (4D). We compare estimates of the critical exponent ν obtained by finite-size scaling analysis of the numerical simulations with the results of the resummation method. Our results show the ability of this Borel-Padé analysis to give quantitative predictions of critical exponents ν for the BdG classes beyond 2D.

The rest of the paper is organized as follows. In Sec. II, we briefly review the Borel-Padé resummation. In Sec. III, we apply the Borel-Padé method to the ϵ series of the critical exponent ν for the BdG classes. In Sec. IV, we apply the Borel-Padé method to the ϵ series of the β functions. In Sec. V, we report our numerical simulations. In Sec. VI, we compare the Borel-Padé predictions with numerical results (both those reported here and previously published work). A summary is given in Table V. In Sec. VII, we discuss and conclude our findings.

II. BOREL-PADÉ RESUMMATIONS

In the scaling theory of Anderson transition [3], the β function is defined as

$$\beta(g) = \frac{d \ln g}{d \ln L}, \tag{6}$$

where g is the dimensionless conductance measured in units of e^2/h and summed over the spins, and L is the length of a d-dimensional cubic system. For the NLσM description, it is more convenient to work with the inverse conductance $t = 1/(\pi g)$ and

$$\beta(t) = -\frac{dt}{d \ln L} = \frac{\beta(g)}{\pi g}. \tag{7}$$

The critical point $t_c > 0$ of the AT is a zero-crossing point of $\beta(t)$,

$$\beta(t_c) = 0, \tag{8}$$

and the critical conductance is given by $g_c = 1/(\pi t_c)$. The critical exponent ν is related to the derivative of the β function at the critical point,

$$\left.\frac{d\beta(t)}{dt}\right|_{t=t_c} = -\left.\frac{d\beta(g)}{d \ln g}\right|_{g=g_c} = -\frac{1}{\nu}. \tag{9}$$

The β functions of the BdG classes up to the 4-loop order [4,45,51] are listed in Table I. Note that the coefficient of t^5

TABLE I. List of the BdG symmetry classes and their transformation behavior under time-reversal, particle-hole, chiral (sublattice) (SLS) symmetries, and the presence (△) or absence (×) of SU(2) spin-rotation symmetry. The penultimate column shows the corresponding noncompact fermionic replica nonlinear sigma-model (NLσM) manifolds. The last column shows the β function [4,45,51] of the four BdG symmetry classes. Here, ζ is the Riemann zeta function.

Class	TRS	PHS	SLS	SU(2)	NLσM manifold	$\beta(t)$ function
D	0	+1	0	×	Sp(2N)/U(N)	$\epsilon t + t^2 - 2t^3 + \frac{7}{2}t^4 - \frac{47}{6}t^5 + O(t^6)$
C	0	−1	0	△	O(2N)/U(N)	$\epsilon t - 2t^2 - 8t^3 - 28t^4 - \frac{376}{3}t^5 + O(t^6)$
DIII	−1	+1	1	×	Sp(2N)	$\epsilon t + t^2 - \frac{1}{2}t^3 + \frac{3}{8}t^4 - \frac{1}{8}\left[\frac{19}{6} + 6\zeta(3)\right]t^5 + O(t^6)$
CI	+1	−1	1	△	O(N)	$\epsilon t - 2t^2 - 2t^3 - 3t^4 - 2\left[\frac{19}{6} + 6\zeta(3)\right]t^5 + O(t^6)$

for class C in Table I differs from that given in Table III of Ref. [4].[1] We also note in passing that the β functions of the chiral symmetry classes were found to be strictly zero in all orders in perturbation theory [52,53].

The Borel-Padé resummation method is a technique for dealing with truncated and possibly divergent series. Given an infinite series f,

$$f(x) = \sum_k f_k x^k, \tag{10}$$

its Borel sum is defined as

$$\tilde{f}(x) = \sum_k \frac{f_k}{k!} x^k. \tag{11}$$

The original series in Eq. (10) can be recovered by calculating the Borel transform,

$$f(x) = \frac{1}{x}\int_0^\infty e^{-y/x}\tilde{f}(y)dy. \tag{12}$$

Suppose the coefficients f_k are known for the order of $k \leqslant l$. We approximate $\tilde{f}$ on the right-hand side by a rational function,

$$\tilde{f}(x) \approx r(x) = \frac{p(x)}{q(x)}, \tag{13}$$

where $p(x)$, $q(x)$ are polynomials of order m and n, respectively,

$$p(x) = \sum_{k=0}^{m} p_k x^k, \qquad q(x) = \sum_{k=0}^{n} q_k x^k, \ q_0 \equiv 1. \tag{14}$$

For choices of $[m, n]$ that satisfy $m + n = l$, the coefficients of the polynomials p and q are uniquely determined. In some cases, we require $m < n$ so that the Padé approximant satisfies

$$\lim_{x\to\infty} r(x) = 0. \tag{15}$$

Then, the rational function r can be decomposed into a sum of partial fractions,

$$r(x) = \sum_{j=1}^{n} \frac{a_j}{x - \lambda_j}, \tag{16}$$

where λ_j are the roots of the polynomial $q(x)$. In general, the λ_j and a_j are complex numbers. Substituting the above equation into Eq. (12) and performing the integration, we obtain the Borel-Padé approximation F of the series for f,

$$F(x) = \frac{1}{x}\sum_{j=1}^{n} a_j B\left(\frac{\lambda_j}{x}\right). \tag{17}$$

Here, the function B is defined by

$$B(s) = \begin{cases} -\exp(-s)E_i(s), & s \in \mathbb{R}, s \neq 0, \\ \exp(-s)E_1(-s), & s \in \mathbb{C}, \arg s \neq \pi, \end{cases} \tag{18}$$

where

$$E_i(x) = -\int_{-x}^{\infty} \frac{e^{-t}}{t}dt = \int_{-\infty}^{+x} \frac{e^t}{t}dt,$$
$$E_1(z) = \int_z^\infty \frac{e^{-t}}{t}dt, \quad |\arg z| < \pi. \tag{19}$$

III. RESUMMATION OF THE SERIES FOR $\nu(\epsilon)$

Series in powers of ϵ for the critical exponent ν can be derived starting from the series for the β function in powers of t as follows. We take symmetry class C as an example. We first find an approximation for $t_c(\epsilon)$ by solving Eq. (8) using the available terms in the power series for $\beta(t)$. For class C, we find

$$t_c(\epsilon) = \frac{1}{2}\epsilon - \epsilon^2 + \frac{9}{4}\epsilon^3 - \frac{77}{12}\epsilon^4 + O(\epsilon^5). \tag{20}$$

Here we have chosen the root for which

$$\lim_{\epsilon\to 0} t_c = 0. \tag{21}$$

[1]We use the value $-376/3$ for the coefficient of t^5 for class C, whereas in Table III of Ref. [4] it is $-376/48$. We believe the latter is a typo and that the coefficient $c_3(-2N)$ should be replaced by $16c_3(-2N)$ so that the β-functions of classes D and C satisfy the duality relation $\beta_{\rm Sp}(t) = -2\beta_{\rm O}(-t/2)$ of the underlying NLσM manifolds. The β-function of class D, which corresponds to the NLσM manifold Sp(2N)/U(N), is given in Eq. (3.7) of Ref. [51]. We thank Alexander D. Mirlin for private communication.

TABLE II. Comparison of the critical exponents ν for classes C and CI in 3D and 4D obtained from Borel-Padé resummations of the series for $\nu(\epsilon)$ when imposing different limiting conditions, i.e., Eq. (26) compared with Eq. (4). Numbers in the square brackets indicate the orders of polynomials, m and n [Eq. (14)].

(a) 3D	$\lim_{d\to\infty}\nu=0$		$\lim_{d\to\infty}\nu=\frac{1}{2}$	
class	[0,3]	[1,2]	[0, 3]	[1,2]
C	0.357	0.227	0.773	0.360
CI	0.555	0.776	0.924	1.226
(b) 4D	$\lim_{d\to\infty}\nu=0$		$\lim_{d\to\infty}\nu=\frac{1}{2}$	
class	[0,3]	[1,2]	[0, 3]	[1,2]
C	0.111	−0.050	0.580	0.527
CI	0.185	0.329	0.633	0.876

If we then substitute the series for t_c into Eq. (9), we obtain the following series in powers of ϵ for the inverse of ν:

$$\nu^{-1}(\epsilon)=\epsilon+2\epsilon^2-\epsilon^3+\frac{15}{2}\epsilon^4+O(\epsilon^5). \tag{22}$$

Taking the reciprocal of this series, we obtain

$$\nu(\epsilon)=\frac{1}{\epsilon}-2+5\epsilon-\frac{39}{2}\epsilon^2+O(\epsilon^3). \tag{23}$$

Similarly, for symmetry class CI, we find

$$\begin{aligned} t_c(\epsilon)&=\frac{1}{2}\epsilon-\frac{1}{4}\epsilon^2+\frac{1}{16}\epsilon^3-\frac{1+9\zeta(3)}{24}\epsilon^4+O(\epsilon^5),\\ \nu^{-1}(\epsilon)&=\epsilon+\frac{1}{2}\epsilon^2+\frac{1}{4}\epsilon^3+\frac{5+36\zeta(3)}{16}\epsilon^4+O(\epsilon^5),\\ \nu(\epsilon)&=\frac{1}{\epsilon}-\frac{1}{2}-\frac{3+36\zeta(3)}{16}\epsilon^2+O(\epsilon^3). \end{aligned} \tag{24}$$

This approach works for symmetry classes C and CI because the coefficient of the t^2 term in $\beta(t)$ is negative and the lower critical dimensions for these classes is $d_l=2$. However, for symmetry classes D and DIII, the coefficient of the t^2 term in $\beta(t)$ is positive, so that when we follow the procedure explained above, we find

$$\lim_{\epsilon\to 0} t_c\neq 0, \tag{25}$$

and we are unable to obtain a useful series in powers of ϵ for ν. This reflects the possibility that the lower critical dimensions for these two classes is below 2D ($d_l<2$), as thought to be the case for the symplectic class AII.

Now we apply the Borel-Padé resummation introduced in the previous section. A naive resummation tacitly assumes the limiting behavior

$$\lim_{d\to\infty}\nu=0, \tag{26}$$

which disagrees with self-consistent theories of the AT and the results for the AT on the Bethe lattice, i.e., with Eq. (4). Instead, we rewrite

$$\nu(\epsilon)=\frac{1}{2}+\frac{1}{\epsilon}f(\epsilon), \tag{27}$$

and perform the resummation of $f(\epsilon)$ with the requirement $m<n$. Such a treatment guarantees the limiting behavior given in Eq. (4). Of course, the application of this restraint to the BdG symmetry classes needs to be justified. For later reference, in Table II, we compare the results given by imposing Eq. (4) and Eq. (26) for the classes C and CI in 3D and 4D.

TABLE III. Lower critical dimension of the BdG symmetry classes D and DIII obtained from the β function without resummation and with order $[m,n]$ Borel-Padé resummation.

Class	No resummation	Borel-Padé	
		[0,4]	[1,3]
D	1.85	1.88	1.76
DIII	1.66	1.70	1.21

IV. RESUMMATION OF THE SERIES FOR $\beta(t)$

An alternative to the approach above is to apply the Borel-Padé method directly to the series for the β function.[11]. All the series take the form

$$\beta(t)=\epsilon t-tf(t), \tag{28}$$

where f is a power series in t. In terms of $f(t)$, the critical exponent is

$$\frac{1}{\nu}=t\frac{df(t)}{dt}\Big|_{t=t_c}. \tag{29}$$

We need to impose the limiting behavior at infinite dimension given in Eq. (4). We first note that in high dimensions, the Anderson transition takes place at strong disorder and, moreover, that

$$\lim_{d\to\infty} t_c=\infty. \tag{30}$$

This means that we can obtain the correct limiting behavior by arranging that

$$\lim_{t\to\infty} t\frac{df}{dt}=A, \tag{31}$$

with $A=2$. To do so, we define h, a polynomial in t, by

$$h(t)=t\frac{df(t)}{dt}-A. \tag{32}$$

Applying the Borel-Padé method to h, we obtain an approximation H for h that satisfies

$$\lim_{t\to\infty} H(t)=0, \tag{33}$$

so that Eq. (31) is satisfied. To obtain the corresponding approximation F for f, a further integration is needed,

$$f(t)\approx F(t)=\int_0^t\frac{A+H(t)}{t}dt. \tag{34}$$

The result can be expressed in the form [11]

$$F(t)=\sum_{j=1}^{n} c_j B(\lambda_j/t),\quad c_j=\frac{a_j}{\lambda_j}. \tag{35}$$

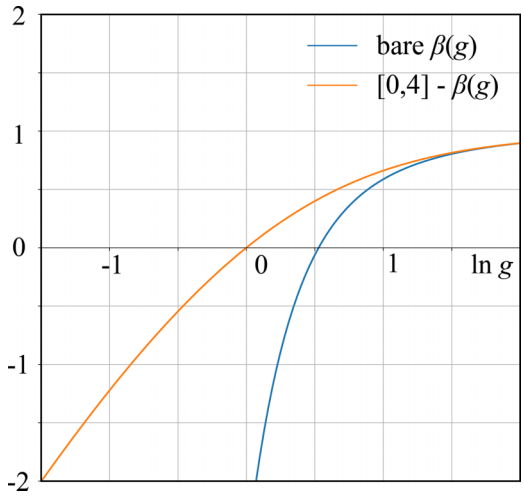

FIG. 1. Comparison of the approximations for the $\beta(g)$ function before and after Borel-Padé resummation of the series for class C in 3D. Numbers in the square brackets indicate the orders of polynomials, m and n [Eq. (14)].

Finally, the β function is approximated as

$$\beta(t) \approx \epsilon t - tF(t). \tag{36}$$

We show the resulting Borel-Padé approximations for $\beta(g)$ in 3D for classes C and CI in Figs. 1 and 2, respectively, together with the series without resummation. We omit the $[m, n] = [1, 3]$ resummation for class C because the resulting β function is not monotonic and has two unphysical fixed points. The limiting behavior $\beta(g) \sim 2 \ln g$ at $g \ll 1$ guaranteed by the constraint $A = 2$ in Eq. (31) is observed only at $\ln g$, much smaller than the range plotted in Fig. 1.

We show the resulting Borel-Padé approximations for $\beta(g)$ in 2D for classes D and DIII in Figs. 3 and 4, respectively, together with the series without resummation. In classes D and DIII, for $d < 2$, two fixed points appear: a critical fixed point and a stable fixed point. At the lower critical dimension

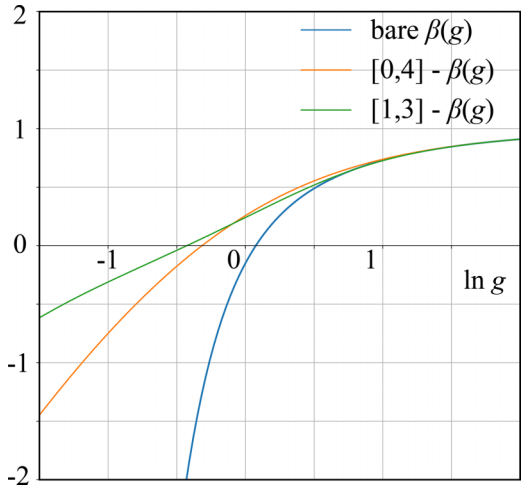

FIG. 2. Comparison of the approximations for the $\beta(g)$ function before and after Borel-Padé resummation of the series for class CI in 3D.

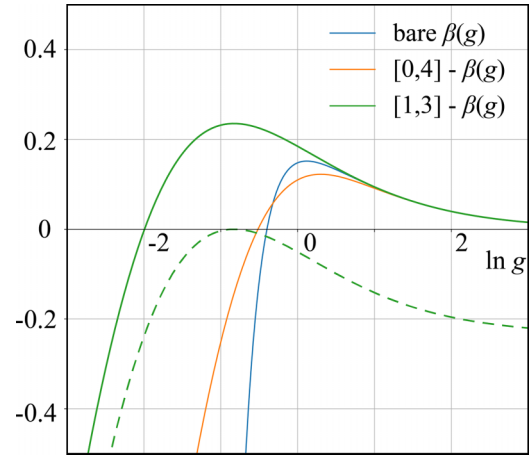

FIG. 3. Comparison of the approximations for the $\beta(g)$ function before and after Borel-Padé resummation of the series for class D in 2D. The [1,3] Bore-Padé resummation of the $\beta(g)$ function at the corresponding estimate $d_l = 1.76$ of the lower critical dimension is plotted with a dashed line.

d_l, these two fixed points annihilate, e.g., the dashed curve in Figs. 3 and 4, and the value of the β function at its maximum is zero,

$$\max_{d=d_l} \beta(g) = 0. \tag{37}$$

This leads directly to an estimate for d_l,

$$d_l \approx 2 - \max \beta(g, \epsilon = 0). \tag{38}$$

Estimates of the lower critical dimension obtained from the Borel-Padé resummations are summarized in Table III.

V. NUMERICAL SIMULATIONS

To evaluate the effectiveness of the Borel-Padé resummation in estimating the critical exponents of the BdG symmetry

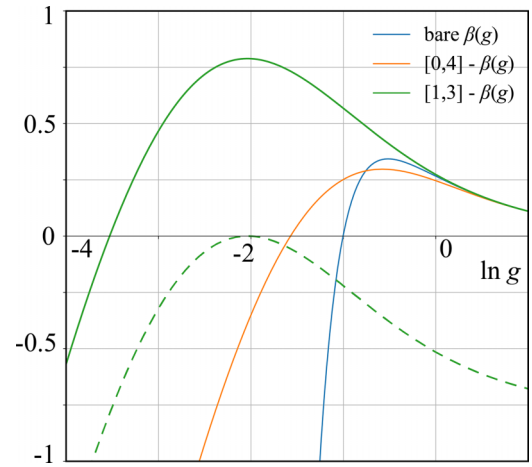

FIG. 4. Comparison of the approximations for the $\beta(g)$ function before and after Borel-Padé resummation of the series for class DIII in 2D. The [1,3] Bore-Padé resummation of the $\beta(g)$ function at the corresponding estimate $d_l = 1.21$ of the lower critical dimension is plotted with a dashed line.

classes, especially in high spatial dimensions $d \geqslant 3$, we perform simulations for 3D class DIII, 4D class C, and 4D class CI. We set the energy E to the particle-hole symmetric point, $E = 0$, and vary the disorder strength W.

A. 3D class DIII

This symmetry class describes time-reversal symmetric superconductors with broken spin-rotational symmetry. We study a four-band tight-binding model on a cubic lattice [54,55],

$$\begin{aligned}\mathcal{H}_{\mathrm{DIII}} &= \sum_{\mathbf{r},\mathbf{r}'} c_{\mathbf{r}}^{\dagger}[H_{\mathrm{DIII}}]_{\mathbf{r}\mathbf{r}'}c_{\mathbf{r}'} \\ &= \sum_{\mathbf{r}}\sum_{\mu=1}^{3}\left[\frac{it}{2}c_{\mathbf{r}+\mathbf{e}_\mu}^{\dagger}\alpha_\mu c_{\mathbf{r}} - \frac{m_2}{2}c_{\mathbf{r}+\mathbf{e}_\mu}^{\dagger}\beta c_{\mathbf{r}} + \mathrm{H.c.}\right] \\ &\quad + \sum_{\mathbf{r}}(m_0 + 3m_2 + v_{\mathbf{r}})c_{\mathbf{r}}^{\dagger}\beta c_{\mathbf{r}}, \end{aligned} \tag{39}$$

where $c_{\mathbf{r}}^{\dagger}$ ($c_{\mathbf{r}}$) is the four-component creation (annihilation) operator on a cubic-lattice site $\mathbf{r}$. For convenience, we set the lattice constant a to be unity. The $\mathbf{e}_{\mu=1,2,3}$ are the primitive lattice vectors along the x, y, z directions, respectively. The matrices α_μ and β are defined as

$$\alpha_\mu = (\sigma_u \otimes \tau_1), \quad \beta = (\sigma_0 \otimes \tau_3), \tag{40}$$

where σ_μ and τ_μ are Pauli matrices acting on different degrees of freedom (e.g., spin and orbital). Parameter m_0 is a mass, and parameters m_2 and t are hopping amplitudes. This Hamiltonian has time-reversal symmetry $U_T^{\dagger} H_{\mathrm{DIII}}^{*} U_T = H_{\mathrm{DIII}}$, where

$$U_T = \delta_{\mathbf{r}\mathbf{r}'}(\sigma_2 \otimes \tau_0), \quad U_T^T = -U_T, \tag{41}$$

and a particle-hole symmetry $U_S^{\dagger} H_{\mathrm{DIII}} U_S = -H_{\mathrm{DIII}}$, where

$$U_S = \delta_{\mathbf{r}\mathbf{r}'}(\sigma_0 \otimes \tau_2). \tag{42}$$

This model depicts a 3D $\mathbb{Z}$ topological superconductor (TSC) when $m_0 < 0$ and a trivial insulator when $m_0 > 0$.

For numerical calculations, we specify the parameters $t = 2, m_2 = 1, m_0 = -2.5$, and use independent uniform distributions for the random on-site potential,

$$v_{\mathbf{r}} \in [-W/2, W/2], \quad \langle v_{\mathbf{r}} v_{\mathbf{r}'}\rangle = \delta_{\mathbf{r}\mathbf{r}'}W^2/12. \tag{43}$$

Here, $\langle\cdot\rangle$ indicates a disorder average. We use the transfer matrix method to calculate the localization length of the model [40] and impose periodic boundary conditions in the transverse direction. We simulate a semi-infinite bar with a cross section of size $L \times L$ and estimate the quasi-one-dimensional (Q1D) localization length λ at disorder strength W and linear size L. A dimensionless ratio Λ is defined as

$$\Lambda(W, L) = \lambda(W, L)/L. \tag{44}$$

The results are shown in Fig. 5, where Λ is plotted versus W for various L. Curves for different L have an approximate common crossing point. This point indicates the Anderson transition between the TSC (localized) phase and the metallic (extended) phase.

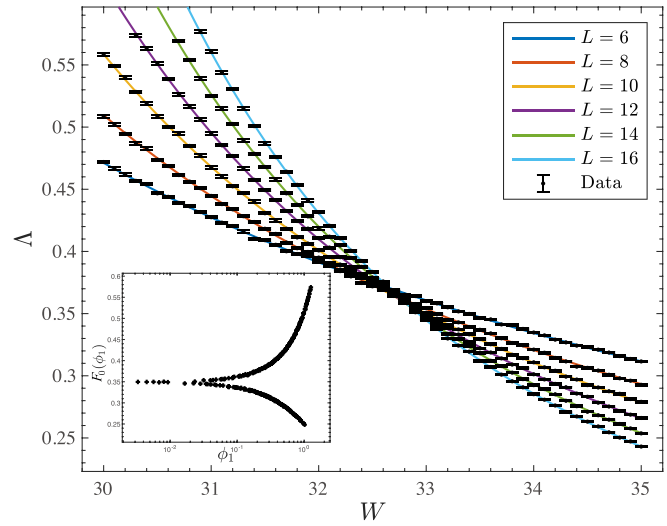

FIG. 5. The dimensionless Q1D localization length Λ near the Anderson transition for the 3D class DIII model. The expansion order is $(n_1, n_2) = (3, 1)$, $(m_1, m_2) = (2, 0)$, as defined in Eqs. (47) and (48). The solid lines are the fitting functions and the black dots with error bars are simulation data points. Inset: the lowest order of the scaling function extracted from the fitting results.

To estimate the critical exponent, we fit the data to the following scaling form that includes corrections to single-parameter scaling due to an irrelevant scaling variable [40,56]:

$$\Lambda = F(\phi_1, \phi_2) = F[u_1(w)L^{1/\nu}, u_2(w)L^{-y}], \tag{45}$$

where

$$\omega = (W - W_c)/W_c, \tag{46}$$

and $\phi_1 = u_1 L^{1/\nu}$ is the relevant scaling variable that encodes the power-law divergence of correlation length $\xi \sim |u_1(w)|^{-\nu}$ around the critical point. The second scaling variable $\phi_2 = u_2 L^{-y}$ with exponent $-y < 0$ is the leading irrelevant correction and vanishes in the limit $L \to \infty$. We approximate the scaling function F using a truncated Taylor series near the critical point ($|w| \ll 1$),

$$F(\phi_1, \phi_2) = \sum_{j=0}^{n_2} F_j(\phi_1)\phi_2^j = \sum_{i=0}^{n_1}\sum_{j=0}^{n_2} f_{ij}\phi_1^i\phi_2^j \tag{47}$$

and

$$u_1 = \sum_{k=1}^{m_1} b_k w^k, \quad u_2 = \sum_{k=0}^{m_2} c_k w^k. \tag{48}$$

We set $b_1 = c_0 = 1$ to remove the arbitrariness of the expansion coefficients. The numerical data are fitted to the scaling function by minimizing the χ-squared statistic,

$$\chi^2 = \sum_{n=1}^{N_{\mathrm{D}}} \frac{(\Lambda_n - F_n)^2}{\sigma_n^2}. \tag{49}$$

Here, N_{D} is the number of data points, Λ_n is the value of Λ for nth data point, σ_n its standard error, and F_n the value of the scaling function for the nth data point. To assess whether or not the fit is acceptable, we use the goodness of fit probability.

TABLE IV. Fitting results for class DIII in 3D, and classes C and CI in 4D. The orders of the expansion of the scaling function are fixed at $n_1 = 3$ and $n_2 = 1$. Here, m_1 and m_2 and the orders, respectively, of the expansions of u_1 and u_2 [see Eqs. (47) and (48)]. The values enclosed in square brackets are 95% confidence intervals determined from 1000 Monte Carlo samples.

(a) 3D class DIII

L	m_1	m_2	GoF	W_c	ν	y	Λ_c
4–16	2	0	0.19	32.909 [32.882, 32.935]	0.972 [0.958, 0.986]	2.09 [1.94, 2.25]	0.349 [0.347, 0.351]
	3	0	0.42	32.903 [32.877, 32.933]	0.981 [0.966, 0.994]	2.14 [1.95, 2.30]	0.350 [0.347, 0.352]
6–16	2	0	0.50	32.917 [22.642, 22.727]	0.952 [0.928, 0.974]	1.98 [1.62, 2.50]	0.349 [0.345, 0.352]
	3	0	0.60	32.898 [32.854, 32.965]	0.963 [0.917, 0.979]	2.23 [1.50, 2.94]	0.351 [0.343, 0.354]

(b) 4D class C

L	m_1	m_2	GoF	W_c	ν	y	g_c
4–12	2	0	0.40	22.65 [22.62, 22.69]	0.724 [0.698, 0.750]	1.45 [1.26, 1.69]	0.83 [0.78, 0.89]
	3	0	0.49	22.66 [22.62, 22.70]	0.724 [0.699, 0.751]	1.45 [1.27, 1.71]	0.83 [0.78, 0.89]
6–12	2	0	0.44	22.68 [22.64, 22.73]	0.698 [0.649, 0.734]	1.66 [1.22, 2.46]	0.80 [0.74, 0.85]
	3	0	0.48	22.68 [22.64, 22.72]	0.703 [0.652, 0.742]	1.61 [1.18, 2.29]	0.80 [0.75, 0.86]

(c) 4D class CI

L	m_1	m_2	GoF	W_c	ν	y	g_c
4–12	2	1	0.97	22.53 [22.50, 22.55]	0.820 [0.710, 0.936]	1.57 [1.48, 1.66]	0.90 [0.88, 0.91]
	3	1	0.98	22.53 [22.51, 22.56]	0.817 [0.722, 0.900]	1.59 [1.50, 1.70]	0.89 [0.88, 0.91]
6–12	3	0	0.93	22.62 [22.58, 22.66]	0.818 [0.713, 0.877]	1.81 [1.55, 2.23]	0.83 [0.81, 0.85]

Here, this is well approximated by [40]

$$\mathrm{GoF} \approx 1 - \frac{1}{\Gamma(N_\mathrm{F}/2)} \int_0^{\chi^2_{\min}/2} dt\, e^{-t}\, t^{\chi^2_{\min}/2-1}, \tag{50}$$

where $N_\mathrm{F} = N_\mathrm{D} - N_\mathrm{P}$ is the degrees of freedom (with N_P the number of fitting parameters), $\chi^2_{\min}$ is the minimum value of the χ-squared statistic, and Γ is the Gamma function. The fitting results are shown in Table IV(a). Our estimate of the critical exponent for 3D class DIII is

$$\nu = 0.96 \pm 0.01. \tag{51}$$

B. 4D class C

Symmetry class C describes disordered superconductors with spin-rotational symmetry, but broken time-reversal symmetry. For this symmetry class, the spin quantum Hall effect occurs in two dimensions [57]. We extend the 3D tight-binding model for class C of Ref. [58] to 4D,

$$\begin{aligned}\mathcal{H}_\mathrm{C} &= \sum_{\mathbf{r},\mathbf{r}'} c^\dagger_{\mathbf{r}} [H_\mathrm{C}]_{\mathbf{r}\mathbf{r}'} c_{\mathbf{r}'} \\ &= \sum_{\mathbf{r}} \Bigg[\sum_{\mu=1}^{3} t\, c^\dagger_{\mathbf{r}+\mathbf{e}_\mu} c_{\mathbf{r}} + t_\parallel c^\dagger_{\mathbf{r}+\mathbf{e}_4} c_{\mathbf{r}} \\ &\quad + i t_\perp \Big(c^\dagger_{\mathbf{r}+\mathbf{e}_1} \sigma_1 c_{\mathbf{r}} + \sum_{\mu=2,3} c^\dagger_{\mathbf{r}+\mathbf{e}_\mu} \sigma_2 c_{\mathbf{r}} \Big) + \mathrm{H.c.} \Bigg] \\ &\quad + \sum_{\mathbf{r}} (v_{\mathbf{r}} + \Delta) c^\dagger_{\mathbf{r}} \sigma_3 c_{\mathbf{r}}. \end{aligned} \tag{52}$$

Here, $c^\dagger_{\mathbf{r}}$ is the creation operator on lattice site $\mathbf{r} = (x_1, x_2, x_3, x_4)$ where the two components act on spin, orbital, or Nambu space, depending on the nature of the system. The Hamiltonian has a particle-hole symmetry $U_P^\dagger H_\mathrm{C}^* U_P = -H_\mathrm{C}$, with

$$U_P = \delta_{\mathbf{r}\mathbf{r}'} e^{i\pi \sum_{\mu=1}^{4} \mathbf{r}\cdot\mathbf{e}_\mu} \sigma_2, \quad U_P^T = -U_P. \tag{53}$$

In the clean limit, the Fourier transformation of the Hamiltonian is

$$\begin{aligned} h_\mathrm{C}(\boldsymbol{k}) &= 2t_\parallel \cos k_4 + 2t \sum_{\mu=1}^{3} \cos k_\mu + \Delta\sigma_3 \\ &\quad - 2t_\perp [\sin k_1 \sigma_1 + (\sin k_2 + \sin k_3)\sigma_2]. \end{aligned} \tag{54}$$

For numerical simulations, we set $\Delta = 0.5$, $t_\perp = t = 1$, and $t_\parallel = 0.8$ so that the clean system has a finite Fermi surface at $E_F = 0$. We calculate the two-terminal Landauer conductance G using the transfer matrix method [59],

$$G = \frac{e^2}{h} g, \quad g = \mathrm{Tr}[\tilde{t}^\dagger \tilde{t}], \tag{55}$$

where $\tilde{t}$ is the transmission matrix of the hypercubic samples of size L^4 along the w axis. We impose periodic boundary conditions in directions that are transverse to the current. While the dimensionless conductance g exhibits fluctuations, various disorder averages are well described by a scaling function like Eq. (45) [60,61]. We calculate $\ln\langle g\rangle$ and use the same nonlinear fitting procedures as described through Eqs. (45)–(50). The numerical data and fitting results are shown in the left panel of Fig. 6. Each data point $\langle g\rangle$ is averaged over 5000–20 000 samples to ensure a relative error smaller than 1%. The results for the critical exponent ν and other quantities are shown in Table IV(b). The fitting results are stable against change of expansion order m_1, m_2 and the range of system size. Our estimate of the critical exponent for 4D class C is

$$\nu = 0.72 \pm 0.02. \tag{56}$$

Note that the critical disorder W_c and critical conductance g_c are model dependent, i.e., not universal.

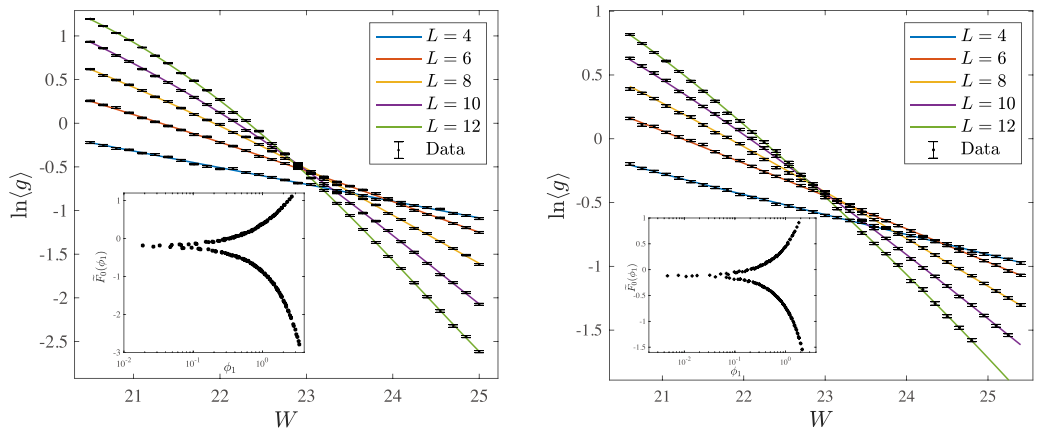

FIG. 6. Dimensionless Landauer conductance as a function of disorder W around the Anderson transition. The expansion order is $(n_1, n_2, m_1, m_2) = (3, 1, 2, 0)$. Left panel: 4D symmetry class C. Right panel: 4D symmetry class CI. The colored solid lines are fitting functions and black dots with error bars are the numerical data. Insets: the lowest order of the scaling function extracted from the fitting results.

C. 4D class CI

Symmetry class CI describes disordered superconductors with both time-reversal symmetry and spin-rotational symmetry. Again, we extended the 3D class CI model of Ref. [58] to 4D,

$$\begin{aligned} H_{\rm CI} &= \sum_{\mathbf{r},\mathbf{r}'} c^\dagger_{\mathbf{r}}[H_{\rm CI}]_{\mathbf{r}\mathbf{r}'}c_{\mathbf{r}'} \\ &= \sum_{\mathbf{r}}\Bigg[\sum_{\mu=1}^{3} t_\perp c^\dagger_{\mathbf{r}+\mathbf{e}_\mu}c_{\mathbf{r}} + t_\parallel c^\dagger_{\mathbf{r}+\mathbf{e}_4}\sigma_3 c_{\mathbf{r}} \\ &\quad + t'_\parallel c^\dagger_{\mathbf{r}+\mathbf{e}_4}\sigma_1 c_{\mathbf{r}} + \text{H.c.}\Bigg] + \sum_{\mathbf{r}}(v_{\mathbf{r}}+\Delta)c^\dagger_{\mathbf{r}}\sigma_1 c_{\mathbf{r}}. \end{aligned} \tag{57}$$

The Hamiltonian is time-reversal symmetric since $H^*_{\rm CI} = H_{\rm CI}$, and has particle-hole symmetry $U_P^\dagger H^*_{\rm CI} U_P = -H_{\rm CI}$ given by

$$U_P = \delta_{\mathbf{r}\mathbf{r}'} e^{i\pi\sum_{\mu=1}^{3}\mathbf{r}\cdot\mathbf{e}_\mu}\sigma_2, \quad U_P^T = -U_P. \tag{58}$$

In the clean limit, the Fourier transformation of the Hamiltonian is

$$\begin{aligned} h_{\rm CI}(\boldsymbol{k}) &= 2t_\perp\sum_{\mu=1}^{3}\cos k_\mu + 2t_\parallel\cos k_4\sigma_3 \\ &\quad + (\Delta + 2t'_\parallel\cos k_4)\sigma_1. \end{aligned} \tag{59}$$

In numerical simulations of the two-terminal Landauer conductance, we chose $\Delta = 1.2$, $t_\perp = 1$, and $t_\parallel = t'_\parallel = 0.5$. Following the same procedures as described in the previous section, we estimate the critical exponent ν and other quantities. The results are shown in the right panel of Fig. 6 and in Table IV(b). Our estimate of the critical exponent ν for 4D class CI is

$$\nu = 0.83 \pm 0.04. \tag{60}$$

VI. COMPARISON OF BOREL-PADÉ PREDICTIONS WITH NUMERICAL RESULTS

Referring to Table V, we see that for classes C and CI in both 3D and 4D, the estimates of the critical exponent obtained with the [0,4] Borel-Padé resummations are in good agreement with the numerical estimates. For 3D class D, the discrepancy is relatively large, and even larger for 3D class DIII. These are also the two symmetry classes where $d_l < 2$ (see Table III). In addition, we notice an inconsistency between our estimation of the critical exponent for 3D class DIII, $\nu = 0.96 \pm 0.01$, and that in Ref. [62], $\nu = 0.85 \pm 0.05$. The model used in Ref. [62] is essentially the same as here, but the data set of Ref. [62] is of smaller size and lower

TABLE V. Critical exponents ν of the BdG symmetry classes in 3D and 4D obtained from order $[m, n]$ Borel-Padé resummation of the β function with $A = 2$, and numerical simulations. Here, $*$ indicates the numerical estimates in this paper, whereas $-$ indicates that the value is yet to be determined. We omit the [1,3] resummation with $A = 2$ for class C because the resummed β function is not monotonic and has two unphysical fixed points. This is also the case for $A = 1$.

(a) 3D

	Borel-Padé with $A = 2$		Numerical	
Class	[0,4]	[1,3]	ν	Ref.
C	1.056		0.996 ± 0.012	[58,64]
CI	1.107	1.822	1.17 ± 0.02	[58]
D	0.823	0.858	0.87 ± 0.03	[58]
DIII	0.751	0.674	0.85 ± 0.05	[62]
			0.96 ± 0.01	*

(b) 4D

	Borel-Padé with $A = 2$		Numerical	
Class	[0,4]	[1,3]	ν	Ref.
C	0.714		0.70 ± 0.02	*
CI	0.729	1.103	0.83 ± 0.04	*
D	0.640	0.666		
DIII	0.616	0.589		

TABLE VI. Critical exponents ν of the BdG symmetry classes in 3D and 4D obtained from β-function series without resummation and order $[m, n]$ Borel-Padé resummation with $A = 1$.

(a) 3D			
	No resummation	Borel-Padé with $A = 1$	
Class		[0,4]	[1,3]
C	0.471	1.446	
CI	0.555	1.478	2.131
D	0.187	1.254	1.249
DIII	0.151	1.202	1.088
(b) 4D			
	No resummation	Borel-Padé with $A = 1$	
Class		[0,4]	[1,3]
C	0.200	1.122	
CI	0.217	1.129	1.602
D	0.103	1.075	1.079
DIII	0.091	1.062	1.026

numerical precision. However, we note the possibility that the weak topological indices may change the critical behavior of the Anderson transition [63].

We have resummed the series for the β function in such a way that Eq. (31) is satisfied. This resummation means that in the localized regime, the β function will behave like $A \ln g$ up to a constant. It would then seem more natural to set $A = 1$ rather than $A = 2$. However, the former choice does not yield the correct limiting behavior given by Eq. (4). For reference, we also tabulate the estimates of the critical exponents calculated from the truncated β-function series without resummation and from the Borel-Padé analysis with $A = 1$ in Table VI. Without resummation, we obtain estimates that violate the Chayes inequality $\nu \geqslant 2/d$ [65]. With $A = 1$, the estimates satisfy the Chayes inequality, but are in poorer agreement with the numerical estimates compared with $A = 2$.

VII. SUMMARY AND DISCUSSION

In this paper, we have studied the Anderson transition in the BdG symmetry classes both analytically and numerically. We applied the Borel-Padé resummation method to the known perturbative results for the NLσM to estimate the critical exponents in 3D and 4D. We also reported numerical simulations of class DIII in 3D, and classes C and CI in 4D, and compared the results of the resummation method with the results of the resummations and previously published work. We find that the results of the Borel-Padé analysis provide estimates of the critical exponent, with the numerical estimates provided by the limiting behavior $\lim_{d\to\infty} \nu(d) = 1/2$ is imposed during the resummation. This condition is inspired by the self-consistent theory of the Anderson model and exact results on the Bethe lattice, but the theoretical justification of it in the nonstandard BdG classes awaits future exploration. In principal, the NLσM theory of Anderson localization and its renormalization analysis in $d = 2 + \epsilon$ dimensions are valid only when ϵ is small, i.e., the Anderson transition occurs under weak disorder. Nonetheless, our results show that the perturbative β functions can provide useful information concerning critical properties in 3D and 4D.

The estimations of the critical exponents in BdG symmetry classes based on the Borel-Padé resummation methods with the assumption of infinite upper critical dimension match the numerical results better. This suggests that the upper critical critical dimension d_u may be infinite for the Anderson localization in BdG symmetry classes. Previous theoretical works have argued that in noncompact NLσM, the upper critical dimension is infinite [66,67], which seems to be consistent with the numerical results and estimation of the Borel-Padé resummation method in this work. Further theoretical efforts are needed to confirm these observations.

Recently, it has been pointed out that the NLσM model characterizes the measurement-induced phase transition in quantum circuits [68]. This scenario involves a replica number N equal to 1. The resummation method discussed in this paper is also applicable to that case, allowing for the prediction of critical exponents in quantum circuit systems.

ACKNOWLEDGMENTS

We thank Ryuichi Shindou, Ferdinand Evers, and Alexander D. Mirlin for fruitful discussions. T.W. was supported by the National Basic Research Programs of China (Grant No. 2019YFA0308401) and the National Natural Science Foundation of China (Grants No. 11674011 and No. 12074008). Z.P. was supported by National Natural Science Foundation of China (No. 12147104). T.O. and K.S. were supported by JSPS KAKENHI Grant No 19H00658, and T.O. was supported by JSPS KAKENHI Grant No. 22H05114.

[1] P. W. Anderson, Absence of diffusion in certain random lattices, Phys. Rev. **109**, 1492 (1958).
[2] F. J. Wegner, Electrons in disordered systems. scaling near the mobility edge, Z. Phys. B **25**, 327 (1976).
[3] E. Abrahams, P. W. Anderson, D. C. Licciardello, and T. V. Ramakrishnan, Scaling theory of localization: Absence of quantum diffusion in two dimensions, Phys. Rev. Lett. **42**, 673 (1979).
[4] F. Evers and A. D. Mirlin, Anderson transitions, Rev. Mod. Phys. **80**, 1355 (2008).
[5] A. Altland and M. R. Zirnbauer, Nonstandard symmetry classes in mesoscopic normal-superconducting hybrid structures, Phys. Rev. B **55**, 1142 (1997).
[6] A. P. Schnyder, S. Ryu, A. Furusaki, and A. W. W. Ludwig, Classification of topological insulators and superconductors in three spatial dimensions, Phys. Rev. B **78**, 195125 (2008).
[7] S. Ryu, A. P. Schnyder, A. Furusaki, and A. W. W. Ludwig, Topological insulators and superconductors: Tenfold way and dimensional hierarchy, New J. Phys. **12**, 065010 (2010).

[8] C.-K. Chiu, J. C. Y. Teo, A. P. Schnyder, and S. Ryu, Classification of topological quantum matter with symmetries, Rev. Mod. Phys. **88**, 035005 (2016).

[9] A. M. García-García, Semiclassical theory of the Anderson transition, Phys. Rev. Lett. **100**, 076404 (2008).

[10] J. M. Edge, J. Tworzydło, and C. W. J. Beenakker, Metallic phase of the quantum Hall effect in four-dimensional space, Phys. Rev. Lett. **109**, 135701 (2012).

[11] Y. Ueoka and K. Slevin, Dimensional dependence of critical exponent of the Anderson transition in the orthogonal universality class, J. Phys. Soc. Jpn. **83**, 084711 (2014).

[12] K. Slevin and T. Ohtsuki, Estimate of the critical exponent of the Anderson transition in the three and four-dimensional unitary universality classes, J. Phys. Soc. Jpn. **85**, 104712 (2016).

[13] P. Prelovšek and J. Herbrych, Diffusion in the Anderson model in higher dimensions, Phys. Rev. B **103**, L241107 (2021).

[14] H. J. Mard, J. A. Hoyos, E. Miranda, and V. Dobrosavljević, Strong-disorder approach for the Anderson localization transition, Phys. Rev. B **96**, 045143 (2017).

[15] F. Iglói and C. Monthus, Strong disorder Rg approach—A short review of recent developments, Eur. Phys. J. B **91**, 1 (2018).

[16] X. Luo, Z. Xiao, K. Kawabata, T. Ohtsuki, and R. Shindou, Unifying the Anderson transitions in Hermitian and non-Hermitian systems, Phys. Rev. Res. **4**, L022035 (2022).

[17] S. Sun and S. Syzranov, Interactions-disorder duality and critical phenomena in nodal semimetals, dilute gases and other systems, arXiv:2104.02720.

[18] S. Zhu and S. Syzranov, BCS-like disorder-driven instabilities and ultraviolet effects in nodal-line semimetals, arXiv:2305.00990.

[19] S. Fishman, D. R. Grempel, and R. E. Prange, Chaos, quantum recurrences, and Anderson localization, Phys. Rev. Lett. **49**, 509 (1982).

[20] G. Casati, I. Guarneri, and D. L. Shepelyansky, Anderson transition in a one-dimensional system with three incommensurate frequencies, Phys. Rev. Lett. **62**, 345 (1989).

[21] A. M. García-García and J. Wang, Anderson transition in ultracold atoms: Signatures and experimental feasibility, Phys. Rev. A **74**, 063629 (2006).

[22] J. Wang and A. M. García-García, Anderson transition in a three-dimensional kicked rotor, Phys. Rev. E **79**, 036206 (2009).

[23] J. Chabé, G. Lemarié, B. Grémaud, D. Delande, P. Szriftgiser, and J. C. Garreau, Experimental observation of the Anderson metal-insulator transition with atomic matter waves, Phys. Rev. Lett. **101**, 255702 (2008).

[24] G. Lemarié, J. Chabé, P. Szriftgiser, J. C. Garreau, B. Grémaud, and D. Delande, Observation of the Anderson metal-insulator transition with atomic matter waves: Theory and experiment, Phys. Rev. A **80**, 043626 (2009).

[25] G. Lemarié, B. Grémaud, and D. Delande, Universality of the Anderson transition with the quasiperiodic kicked rotor, Europhys. Lett. **87**, 37007 (2009).

[26] G. Lemarié, H. Lignier, D. Delande, P. Szriftgiser, and J. C. Garreau, Critical state of the Anderson transition: Between a metal and an insulator, Phys. Rev. Lett. **105**, 090601 (2010).

[27] M. Lopez, J.-F. Clément, P. Szriftgiser, J. C. Garreau, and D. Delande, Experimental test of universality of the Anderson transition, Phys. Rev. Lett. **108**, 095701 (2012).

[28] M. Santhanam, S. Paul, and J. B. Kannan, Quantum kicked rotor and its variants: Chaos, localization and beyond, Phys. Rep. **956**, 1 (2022).

[29] D. Vollhardt and P. Wölfle, Diagrammatic, self-consistent treatment of the Anderson localization problem in $d \leqslant 2$ dimensions, Phys. Rev. B **22**, 4666 (1980).

[30] D. Vollhardt and P. Wölfle, Scaling equations from a self-consistent theory of Anderson localization, Phys. Rev. Lett. **48**, 699 (1982).

[31] R. Abou-Chacra, D. J. Thouless, and P. W. Anderson, A self-consistent theory of localization, J. Phys. C **6**, 1734 (1973).

[32] H. Kunz and B. Souillard, The localization transition on the Bethe lattice, J. Phys. Lett. **44**, 411 (1983).

[33] A. D. Mirlin and Y. V. Fyodorov, Localization transition in the Anderson model on the Bethe lattice: Spontaneous symmetry breaking and correlation functions, Nucl. Phys. B **366**, 507 (1991).

[34] A. D. Mirlin and Y. V. Fyodorov, Distribution of local densities of states, order parameter function, and critical behavior near the Anderson transition, Phys. Rev. Lett. **72**, 526 (1994).

[35] A. Klein, Extended states in the Anderson model on the Bethe lattice, Adv. Math. **133**, 163 (1998).

[36] A. De Luca, B. L. Altshuler, V. E. Kravtsov, and A. Scardicchio, Anderson localization on the Bethe lattice: Nonergodicity of extended states, Phys. Rev. Lett. **113**, 046806 (2014).

[37] S. Savitz, C. Peng, and G. Refael, Anderson localization on the Bethe lattice using cages and the Wegner flow, Phys. Rev. B **100**, 094201 (2019).

[38] M. Schreiber and H. Grussbach, Dimensionality dependence of the metal-insulator transition in the Anderson model of localization, Phys. Rev. Lett. **76**, 1687 (1996).

[39] A. M. García-García and E. Cuevas, Dimensional dependence of the metal-insulator transition, Phys. Rev. B **75**, 174203 (2007).

[40] K. Slevin and T. Ohtsuki, Critical exponent for the Anderson transition in the three-dimensional orthogonal universality class, New J. Phys. **16**, 015012 (2014).

[41] F. Wegner, The mobility edge problem: Continuous symmetry and a conjecture, Z. Phys. B **35**, 207 (1979).

[42] L. Schäfer and F. Wegner, Disordered system within orbitals per site: Lagrange formulation, hyperbolic symmetry, and goldstone modes, Z. Phys. B **38**, 113 (1980).

[43] K. Efetov, Supersymmetry and theory of disordered metals, Adv. Phys. **32**, 53 (1983).

[44] S. Hikami, Localization, nonlinear σ model and string theory, Prog. Theor. Phys. Suppl. **107**, 213 (1992).

[45] S. Hikami, Three-loop ß-functions of nonlinear σ models on symmetric spaces, Phys. Lett. B **98**, 208 (1981).

[46] S. Hikami, Anderson localization in a nonlinear-σ-model representation, Phys. Rev. B **24**, 2671 (1981).

[47] S. Hikami, Isomorphism and the β-function of the nonlinear σ model in symmetric spaces, Nucl. Phys. B **215**, 555 (1983).

[48] W. Bernreuther and F. J. Wegner, Four-loop-order β function for two-dimensional nonlinear sigma models, Phys. Rev. Lett. **57**, 1383 (1986).

[49] I. Travěnec and P. Markoš, Critical conductance distribution in various dimensions, Phys. Rev. B **65**, 113109 (2002).

[50] Y. Ueoka and K. Slevin, Borel-Padé resummation of the β-functions describing Anderson localisation in the Wigner-Dyson symmetry classes, J. Phys. Soc. Jpn. **86**, 094707 (2017).

[51] F. Wegner, Four-loop-order β-function of nonlinear σ-models in symmetric spaces, Nucl. Phys. B **316**, 663 (1989).

[52] R. Gade and F. Wegner, The $n = 0$ replica limit of U(n) and U(n)SO(n) models, Nucl. Phys. B **360**, 213 (1991).

[53] R. Gade, Anderson localization for sublattice models, Nucl. Phys., Sec. B **398**, 499 (1993).

[54] C.-X. Liu, X.-L. Qi, H. J. Zhang, X. Dai, Z. Fang, and S.-C. Zhang, Model Hamiltonian for topological insulators, Phys. Rev. B **82**, 045122 (2010).

[55] K. Kobayashi, T. Ohtsuki, and K.-I. Imura, Disordered weak and strong topological insulators, Phys. Rev. Lett. **110**, 236803 (2013).

[56] K. Slevin and T. Ohtsuki, Corrections to scaling at the Anderson transition, Phys. Rev. Lett. **82**, 382 (1999).

[57] V. Kagalovsky, B. Horovitz, Y. Avishai, and J. T. Chalker, Quantum Hall plateau transitions in disordered superconductors, Phys. Rev. Lett. **82**, 3516 (1999).

[58] T. Wang, T. Ohtsuki, and R. Shindou, Universality classes of the Anderson transition in the three-dimensional symmetry classes AIII, BDI, C, D, and CI, Phys. Rev. B **104**, 014206 (2021).

[59] J. B. Pendry, A. Mackinnon, and P. J. Roberts, Universality classes and fluctuations in disordered-systems, Proc. R. Soc. London Ser. A-Math. Phys. Eng. Sci. **437**, 67 (1992).

[60] K. Slevin, P. Markoš, and T. Ohtsuki, Reconciling conductance fluctuations and the scaling theory of localization, Phys. Rev. Lett. **86**, 3594 (2001).

[61] K. Slevin, P. Markoš, and T. Ohtsuki, Scaling of the conductance distribution near the Anderson transition, Phys. Rev. B **67**, 155106 (2003).

[62] B. Roy, Y. Alavirad, and J. D. Sau, Global phase diagram of a three-dimensional dirty topological superconductor, Phys. Rev. Lett. **118**, 227002 (2017).

[63] Z. Xiao, K. Kawabata, X. Luo, T. Ohtsuki, and R. Shindou, Anisotropic topological Anderson transitions in chiral symmetry classes, Phys. Rev. Lett. **131**, 056301 (2023).

[64] M. Ortuño, A. M. Somoza, and J. T. Chalker, Random walks and Anderson localization in a three-dimensional class C network model, Phys. Rev. Lett. **102**, 070603 (2009).

[65] J. T. Chayes, L. Chayes, D. S. Fisher, and T. Spencer, Finite-size scaling and correlation lengths for disordered systems, Phys. Rev. Lett. **57**, 2999 (1986).

[66] A. Codello and R. Percacci, Fixed points of nonlinear sigma models in $d > 2$, Phys. Lett. B **672**, 280 (2009).

[67] A. N. Efremov and A. Rançon, Nonlinear sigma models on constant curvature target manifolds: A functional renormalization group approach, Phys. Rev. D **104**, 105003 (2021).

[68] M. Fava, L. Piroli, T. Swann, D. Bernard, and A. Nahum, Nonlinear sigma models for monitored dynamics of free fermions, arXiv:2302.12820.